Experimental Testing and Model Validation of a Decoupled-Phase On-Load Tap Changer Transformer in an Active Network

Zecchino, Antonio; Hu, Junjie; Coppo, Massimiliano ; Marinelli, Mattia

Published in:
IET Generation Transmission and Distribution

Link to article, DOI:
10.1049/iet-gtd.2016.0352

Publication date:
2016

Document Version
Peer reviewed version

Experimental Testing and Model Validation of a Decoupled-Phase On-Load Tap Changer Transformer in an Active Network

Antonio Zecchino [1*], Junjie Hu [1], Massimiliano Coppo [2], Mattia Marinelli [1]

[1] Department of Electrical Engineering, Technical University of Denmark, Roskilde, Denmark
[2] Department of Electrical Industrial Engineering, University of Padova, Padova, Italy
[*] antozec@elektro.dtu.dk

Abstract: Due to the increasing penetration of single-phase small generation units and electric vehicles connected to distribution grids, system operators are facing challenges related to local unbalanced voltage rise or drop issues, which may lead to a violation of the allowed voltage band. To address this problem, distribution transformers with on-load tapping capability are under development. This paper presents model and experimental validation of a 35 kVA three-phase power distribution transformer with independent on-load tap changer control capability on each phase. With the purpose of investigating and evaluating its effectiveness under different operative conditions, appropriate scenarios are defined and tested considering both balanced and unbalanced situations, also in case of reverse power flow. The experimental setup is built starting from an analysis of a Danish distribution network, in order to reproduce the main feature of an unbalanced grid. The experimental activities are recreated in by carrying out dynamics simulation studies, aiming at validating the implemented models of both the transformer as well as the other grid components. Phase-neutral voltages' deviations are limited, proving the effectiveness of the phase-independent tap operations. Furthermore, minor deviations of the results from simulations and experiments confirm that all the system components have been properly modelled.

1. Introduction

The increasing presence of distributed energy resources (DERs) like photovoltaic (PV) and new storage-capable loads, such as electric vehicles (EVs), may result into non-conventional power flows causing non-monotonic voltage variations along the feeder, with the risk of violating the permitted voltage band [1]–[4]. Due to this, distribution system operators (DSOs) are being forced into grid reinforcement investments, even though the grid capacity is far from exhausted.

To reduce the mentioned voltage issues, many alternatives are proposed. Historically, conservation voltage reduction (CVR) solutions are proposed to reduce electrical demand by maintaining the delivered voltage to the customer in the lower portion of the acceptable range, resulting in reduction of energy consumption over time [5]–[7]. Other recent strategies include voltage control using reactive power provision from PV inverters [3], [4] and [8], active power de-rating of the PV production in case of overvoltage conditions [9], EV smart charging technology [4], [10], distribution static compensator (DSTATCOM) [11] and voltage control at the LV side of the MV/LV transformer by on-load tap changers (OLTC) [12].

Moreover, in [13] and [14] control methods based on coordination of OLTC operations and reactive power exchange between the DSO and PV inverters are studied. The three-phase OLTC technology

applied in secondary substation transformers is feasible and products are available on the market. Several power engineering components manufacturers such as, among others, Maschinenfabrik Reinhausen Gmbh and SIEMENS are offering such devices ([15] and [16]).

However, the reported MV/LV OLTC transformers modulate the voltage evenly on the three-phases, thus not considering the unbalanced conditions in LV feeders. Due to massive presence of single-phase connected DERs, voltage unbalance is becoming more and more an issue that DSOs need to handle.

To address this problem, many inverter-based solutions are proposed in [3], [4] and [8], [17] and [18]. Alternatively, as innovative solution, particular attention is given to the decoupled-phase OLTC technology, which could allow a reduction of the unbalance conditions in distribution grids, as demonstrated in [19] and [20]. In these works, the authors investigated the technology by means of mere simulation studies, by modelling the decoupled-phase OLTC operations in a preliminary simplified way with limited modelling insights of the new technology. A LV distribution grid with the addition of single-phase PV units distributed along the feeder has been considered in [19] and [20]. Simulation results show that with the decoupled-phase OLTC actions, the PV hosting capacity of the grid can be significantly increased, since the unbalance effect has been mitigated. Further positive effects are obtained if also reactive power regulation from single-phase inverters connected to the PVs is performed simultaneously.

As continuation of the mentioned simulation analysis, with this work the authors present the investigation of a real decoupled-phase OLTC transformer manufactured by the German company Schuntermann Transformatoren Gmbh and currently available on the market [21]. The device is a three-phase Delta-Wye transformer which, independently on each phase, allows a regulation of the output voltage of ±10% of the rated voltage (400/230 V for either side). In comparison with the previous works, the here-presented simulation models are enhanced by the outcome of the experimental investigations. These enhancements mainly regard the characterization of the main parameters of the OLTC and the implementation of the real tap operation, which is now non-linear. With the purpose of improving the power quality in terms of voltage unbalance reduction, the unit has been tested in an experimental LV grid. The LV grid is built in a way to reproduce the distribution grid utilized for the former simulation activities. Moreover, the current study focuses on the investigation of the real transformer, not only by means of experimental activities, but also relying on an exhaustive modelling validation in DIgSILENT PowerFactory software environment by carrying out dynamics simulation studies. Based on the preliminary investigation study presented by the authors in [19] and [20] and thanks to the experimental activity discussed in this paper, the proposed transformer model is now consistent with the behaviour of the real device.

The novelty of this work is: 1) the development of a method for experimentally reproducing a real distribution grid in a simplified and reduced-scale experimental facility; 2) an experimental investigation of the decoupled-phase OLTC transformer; 3) the modelling of all the utilized components; and 4) the validation of results from real experiments and simulations.

In Section 2 the experimental system is presented. A modelling in DIgSILENT PowerFactory software environment of all the components involved in the experimental activities is then proposed in Section 3. In Section 4 the OLTC's operability is studied: scenarios characterized by both balanced and unbalanced load conditions as well as by single-phase reverse power flow are defined. Conclusions are reported in Section 5.

2. Experimental System Design and Overview

In this section, firstly the choice of all the utilized components is justified by considering a real Danish low voltage distribution network. Further attention is given to the OLTC as well as to the other system's components.

2.1. Setup Specification through Analysis of a Real Network

The physical setup utilized for the experiments has been built so to reproduce as realistically as possible a reference real Danish LV distribution network, whose data have been provided by Dong Energy, a local DSO. The considered distribution system has already been adopted in the previously presented works dealing with the feasibility of the decoupled-tap-changer approach and its effect on the network ([19] and [20]). In order to define the size of the devices employed in the experimental setup (i.e., OLTC rated power, cable length and impedance, loads power), an analysis of the electrical characteristics of a real system is conducted, in particular with the aim of selecting a suitable cable size (length and section) to represent the line impedance of the reference network.

In Fig. 1 the distribution feeder layout is shown, along with the cables length and impedance. In order to have a simplified setup, this analysis' aim is to calculate an equivalent impedance of the real network. Further, the line sections connecting the MV/LV transformer and the farther busbar (i.e., Bus 12) were considered (highlighted in Fig. 1).

The total impedance for the highlighted line is given by (1) considering the three different cable types employed, described in Fig. 1:

$$Z_{TOT} = \sum_{type=1}^{3} |z_{type}| \cdot L_{type} \quad (1)$$

where $|z_{type}| = |r_{type} + j\, x_{type}|$ is the per-unit-length impedance magnitude [Ω/km] and L_{type} is the total length [km], both associated to each cable type and section. The total impedance Z_{TOT} is then used to calculate an index of the 'impedance density' defined as the ratio between total impedance and total load power:

$$K_Z = \frac{Z_{TOT}}{P_{TOT}} \quad (2)$$

where P_{TOT} is the total load power [kW] calculated as the average consumption of the loads connected to the network, measured during one day operation, and K_Z is defined as 'impedance density' index [Ω/kW]. This index links the impedance magnitude with the active power in a direct proportionality considering the fact that voltage drops in low voltage distribution networks, usually composed by cables with high R/X ratio, depend mainly on the active power flow.

Assuming a total load's three-phase rated power (fixed) and different cable types, the line length for the experimental setup can now be defined through (3) using the impedance density index defined in (2):

$$L_{TEST} = \frac{K_Z \cdot P_{TEST}}{|z_{cable}|} \quad (3)$$

where two of the variables need to be set in accordance with the test: P_{TEST} is the OLTC's rated power [kW] (also defining the loads' size), while $|z_{cable}|$ is the impedance of the cable magnitude [Ω/km] and depends on the type selected for the setup.

In this case, the impedance of the line highlighted in Fig. 1 is 92.64+j36.84 mΩ, while the average load power during one day operation of the network is 31 kW. These values resulted in an impedance density K_Z = 3.22 mΩ/kW. In order to recreate the most realistic network equivalent, the closest size available for the OLTC device is 35 kVA, while the cable chosen for the setup is a 16 mm^2 copper conductor (z_{cable}=1.45+j0.081 Ω/km). By using the K_Z value reported above and with the mentioned z_{cable}, the cable length can be calculated as for Equation (3) adopting P_{TEST} = 35 kW, resulting in 77.5 m.

To verify the accuracy of the analysis, an evaluation of the three-phase short-circuit current has been performed, by simulating a fault at Bus 12 in the real system's model and at the load bus in the equivalent circuit. They amounted respectively to 1626 A and 1638 A. To further validate the correspondence between the original model and the equivalent branch, the voltage drop has been calculated in the two cases imposing a 1 p.u. voltage at the starting bus (i.e., Bus 1 in the network model). For the network model shown in Fig. 1 the only load considered in this test is the one connected at Bus 12, with a power of

31 kW, equal to P_{TOT} in Equation (2), and unitary power factor. The equivalent branch is composed by the cable considered in the calculation above, resulting in the mentioned L_{TEST}. The feeder-end voltage in the two cases (i.e., original network model vs equivalent branch) resulted respectively in 0.982 p.u. and 0.975 p.u., which allows considering acceptable the approximation made in the study, being the error equal to 0.007 p.u..

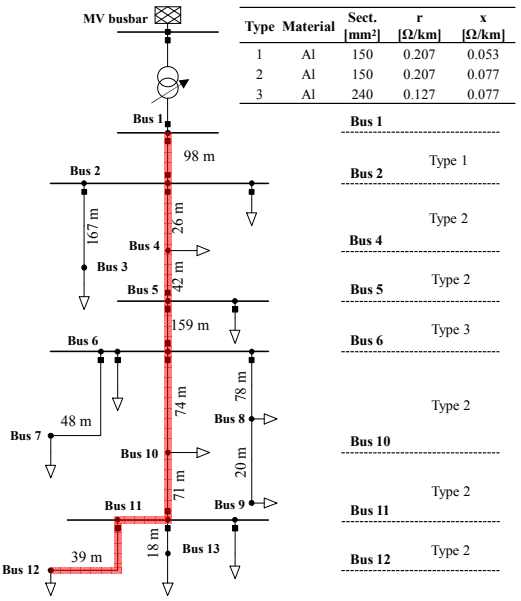

Fig.1. *Danish real distribution feeder layout*

2.2. Experimental Setup

The experimental validation has been performed in the research infrastructure SYSLAB-PowerLabDK, a laboratory facility for the development and test of control and communication technology for active and distributed power systems, located at the DTU Risø campus [22].

As result of the proposed analysis, the basic simplified experimental setup layout has been composed of the 35 kVA decoupled-phase OLTC transformer under investigation, a 16 mm^2 three-phase 75 meter-long copper cable and a resistive load with the feature of independent single-phase power absorption control up to 15 kW per phase.

In addition to the mentioned realistic passive outline, an EV featured with Vehicle-To-Grid (V2G) services provision capability has been connected to the system aiming at representing a single-phase active user connected to the LV grid. It allows grid support by raising the voltage locally, thanks to the possibility of active power injection.

The setup of the experiment is presented in Fig. 2. It can be noticed that two measurement devices have been utilized for monitoring and collecting data. Specifically, they have been installed at the two terminals of the cable, i.e., at the secondary side of the OLTC and at the load/EV bus. In particular, they allow monitoring voltages and currents on the four active wires (the three phases and the neutral conductor) at the two measurement points, both in terms of root-mean-square (RMS) values and of sequence-related indexes. The utilized measurement devices are two 'ELSPEC BlackBox G4500 Power Quality Analyzer' units [23].

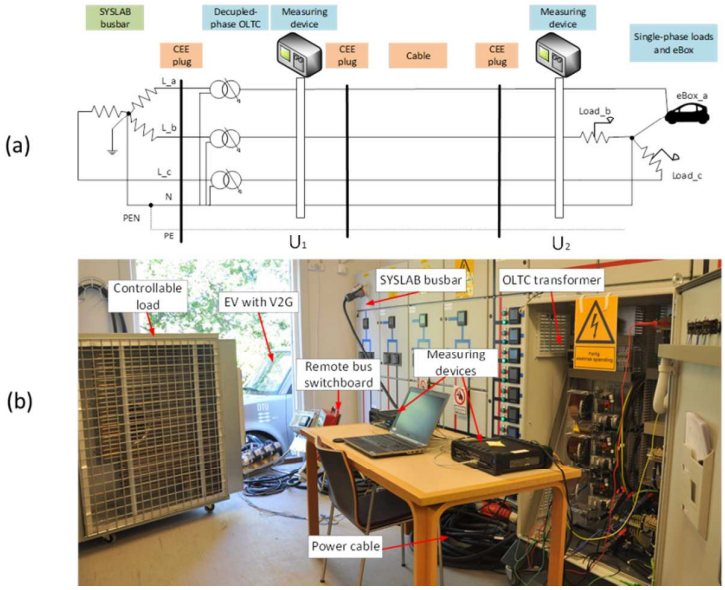

Fig.2. *System layout for the experimental activities*
a. Schematic setup
b. Real setup

2.3. OLTC – Hardware Description

The decoupled-phase OLTC transformer under examination is a three-phase Delta-Wye transformer with the neutral grounded at the secondary side. The rated voltage is 230 V both at the primary (V_{n1}) and at the secondary side (V_{n2}). Independently on each phase at the secondary side, it is possible to have an adjustment range (ΔV_2) of ±10% of the output voltage. In fact, rather than as a standard transformer with up/down voltage level transformation capability, such a unit should be considered as a mere voltage stabilizer for increasing the grid power quality by reducing the phase-neutral voltage deviations. The rated power is 35 kVA, which corresponds to 11.66 kVA for each single-phase unit, while the rated current I_n amounts to 50 A. Fig. 3 shows its internal structure: it is composed by three single-phase toroidal coil transformers equipped with winding selectors connected to three servo motors, whose operations are managed by independent control units according to voltage measurements at the secondary side, obtained

through three single-phase voltage measurement transformers. On the right side, three single-phase booster transformers are placed, whose main function is to split the total power among two steps of transformation, so to reduce the size of the three servo motors.

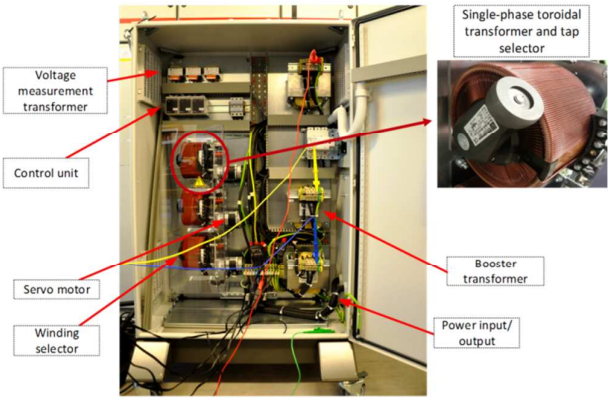

Fig.3. *OLTC transformer internal structure*

The OLTC operates on a closed loop control. Independently on each phase, the output voltage is measured and compared with a reference voltage in the control unit. Whenever it exceeds the allowed dead band *DB* (1% of V_n), tap actions are performed until the dead band is reached again.

With the purpose of investigating the described tap operation, RMS values of phase-neutral voltages at the secondary side have been monitored and analysed while tap activities take place as a consequence of load changes. Firstly, the tap operation scheme depicted in Fig. 4-a has been considered as a reference. It can be noticed that, after the voltage drop ΔV, a delay-time *D1* preventing tap actions due to short-term voltage variations precedes the voltage increase ΔV_{step} caused by the tap action, whose duration has been named T_{step}. Between two consecutive steps, a certain delay-time *D2* has been detected.

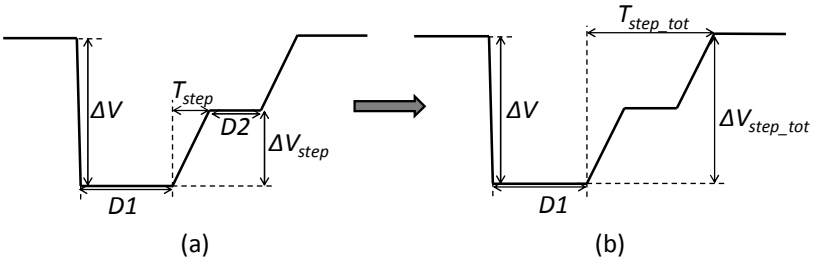

Fig.4. *OLTC tap operation investigation*
a. Firstly considered OLTC operation trend
b. Simplified OLTC operation trend

The zoom in Fig. 3 shows in detail the outline of the toroidal unit where the tap selector is placed, consisting in total of about 400 turns. Results have also shown that every real tap activity is on average

composed by 2 steps ΔV_{step} and that the tap selector concatenates about ±12 turns. Therefore it has been possible to conclude that the voltage difference caused by a single turn is very limited, justifying an inconstancy of the measured ΔV_{step} and delay-times. In fact, test results have shown that both ΔV_{step} and $D1$ are not constant: they assumed values within the ranges 0.5-0.9 V and 60-160 ms, respectively, while $D2$ and T_{step} amounted to 20 or 40 ms. It is important to underline that the sampling time of the measurement device is 20 ms.

As outcome of this operation analysis, it can be concluded that the actual tap actions described by 2 small steps ΔV_{step} could actually be considered as one. Therefore, hereafter it has been decided to consider the behaviour of a single larger tap activity: the reference OLTC operation trend could then be easily simplified as the one reported in Fig. 4-b. In this regard, henceforth two main parameters have been taken into account related to each aggregated tapping action: the total voltage variation ΔV_{step_tot} and the time needed for the whole operation T_{step_tot}. Specifically, as the average value of all the measured ΔV_{step} amounted to 0.72 V, it has been decided to consider values of 1.44 V for ΔV_{step_tot}. Consequently, a total number of steps of 32 (±16 from the '0-position') has been obtained, achieving in this way the expected regulation range ±10% of the rated voltage. Regarding T_{step_tot} and $D1$, the value of 60 ms has been chosen based on the considerations made on the test results.

For a complete investigation of the transformer, in addition to the tap activity operation, also some structural internal parameters needed to be calculated. In this regards, the open-circuit test allowed the determination of both the iron losses P_{iron_loss} and the no-load current $i_{0\%}$: the first one amounted to 15 W, while the second one to 0.18% of the rated current. Although the standard procedure for the characterization of a power transformer includes the short-circuit test, in this study its performance has not been possible due to the lack of availability of an autotransformer able to provide the appropriate short-circuit voltage, i.e., the reduced supply voltage needed for such a test. Therefore, it has been decided to calculate the copper losses P_{Cu} through an indirect procedure shown in (4), as difference of the calculated load-losses under nominal load condition P_{loss_n} and the iron losses P_{iron_loss}, divided by the square of the grade of loading. The grade of loading is defined as the ratio between the current flowing due to a particular load I_{load} and the nominal current I_n and thus takes into account the square dependency to the loading level.

$$P_{Cu}=(P_{loss\_n}-P_{iron\_loss})/(I_{load}/I_n)^2=P_{loss\_n}-P_{iron\_loss} \quad (4)$$

Practically, in the performed tests nominal conditions have been utilized, so that the factor $(I_{load}/I_n)^2$ has been considered equal to 1. In order to find the amount of the on-load losses – from which, the copper losses – for different operative conditions, the on-load test has been repeated for all the possible tap

positions. It has been obtained a linear downward trend from the lowest tap position to the '0-position' (unitary turns ratio), and a symmetrical upward trend to the upper limit. Specifically, at both the extreme positions the copper losses are 85 W ($P_{Cu\_extreme}$), while at the central position they amount to 35 W ($P_{Cu\_central}$), i.e., 0.73% and 0.3% of the rated single-phase unit power, respectively.

2.4. Load – Hardware Description

As discussed in Section 2.2, a custom-made 45 kW (i.e., 15 kW per phase, adjustable with steps of 0.1 kW) load unit equipped with a three-phase CEE 63 A plug for the supply has been utilized. According to the active power independently settable on each phase, appropriate connections of internal resistor branches are provided, so to achieve the necessary resistance, resulting in the desired active power absorption. It is therefore clear that the load is representable with a constant-impedance model, with reference to the ZIP theory [24]. In fact, the unit is manufactured so the set active power P_0 corresponds to the effectively absorbed power P_{eff} just under nominal voltage conditions V_0. Otherwise the effective load power would change with the square of the ratio of the effective supply voltage V_{eff} and the rated one, as in (5).

$$P_{eff}=P_0 \cdot (V_{eff}/V_0)^2 \quad (5)$$

2.5. EV – Hardware Description

The utilized EV is an eBox, a conversion of a Toyota Scion xB vehicle into a battery electric vehicle produced by the U.S. Company AC Propulsion. The eBox is equipped with a 35 kWh battery and a power electronics unit (PEU) capable of single-phase bidirectional power transfer up to 20 kW. It is controllable either by the EV computer that interfaces with the PEU using build-in vehicle smart link (VSL) or directly via the vehicle management system (VMS) [25].

In this case, the VMS has been utilized. It allows the manual adjustment of the injected/absorbed current – limited to 16 A due to the technical limitation of the single/three-phase switchboard, which the EV is connected to. Therefore, for the performed experimental tests, the set current has been considered as reference value for the analysis of the operative scenarios. Again with reference to [24], the EV is representable with a 'constant-current' model, meaning that its behaviour is characterized by a constant ratio of active power and voltage. Therefore it is clear that, unless the operation is run under nominal voltage condition, the injected power P_{eff} would deviate from the nominal power P_0 with the ratio of the effective supply voltage V_{eff} and the rated voltage V_0, according to (6).

$$P_{eff}=P_0 \cdot (V_{eff}/V_0) \quad (6)$$

3. Modelling of the Experimental System Elements

All the elements involved in the practical tests have been modelled in DIgSILENT PowerFactory software environment, with the aim of reproducing as realistically as possible their operational behaviour during the experiments. In the following sections the modelling is presented.

3.1. OLTC – Modelling

In order to perform independent single-phase changes of the transformation ratios in the simulation tool, the real OLTC Dyn transformer has been modelled with three single-phase units independently controlled, whose secondary sides are connected between an earthed neutral point and a different phase of the modelled experimental LV grid. Each single-phase transformer has been set with rated power P_n of 11.66 kVA and characterized by a regulation capability of ±10% of the rated voltage at the secondary side.

With the aim of representing the investigated tap activity reported in Fig. 4-b, two blocks have been built to model the control scheme, shown in Fig. 5. The first one calculates the deviation ΔV of the measured local voltage V_{meas} from the reference voltage V_{ref}, which is manually set as input value. According to size and sign of ΔV, two appropriate internal parameters *check* and *sign* assume respectively values of 0/+1 or -1/+1. They aim both at activating the tap action – whenever the deviation exceeds half of the allowed dead band set at 1% of the rated voltage – and at deciding whether the turns ratio needs to be increased or decreased. If the calculated new tap position *newtap* overcomes the allowed extreme tap positions (±16), then ±16 is provided as output. The output of the first block is so delayed by 120 ms by the second block, a simple delay-block which includes both the intentional delay-time *D1* and the operational time T_{step_tot} described in Section 2.3, in order to guarantee the total effective time needed by the transformer for a physical tap operation. The obtained delayed tap position is both applied to the transformer unit and utilized as retro-input for the next simulation step. The 3 tap-changing devices operate independently, referring each one to the respective single-phase voltage measurement.

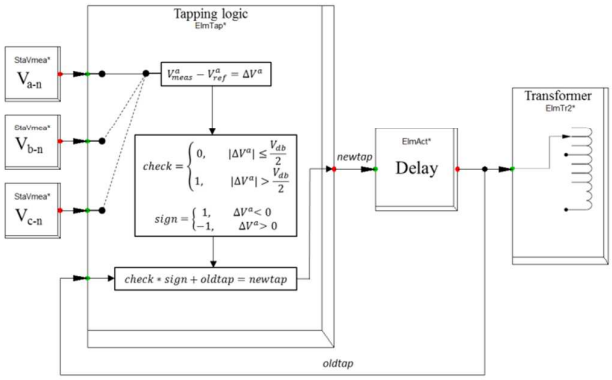

Fig.5. *Control scheme for the decoupled-phase OLTC transformer*

For a complete and realistic representation of the transformer, iron losses, no-load current and copper losses have been set according to the results presented in Section 2.3. Another required internal parameter is the short-circuit voltage V_k, which, as explained above, could not be calculated. It has therefore been set arbitrarily to 4% of the rated voltage, according to the realistic value utilized in the previously mentioned simulation works [19] and [20]. It is important to state that the choice of an arbitrary value of V_k does not significantly influence the results of the performed investigation. In fact, it would mainly influence only in case of loads with cosφ far from unitary value, since the short circuit impedance is mainly inductive. In the analysed cases both the loads and the EV have unitary power factor, leading to the conclusion that the choice of 4% will marginally influence the results.

Table 1 provides an overview of all the modelling parameters of the decoupled-phase OLTC transformer.

Table 1 Overview of all the OLTC transformer modelling parameters

Name	Value	Explanation
V_{n1}	230 V	Nominal voltage at the primary side
V_{n2}	230 V	Nominal voltage at the secondary side
S_n	35 kVA	Nominal apparent power
I_n	50 A	Rated current
ΔV_2	±10% of V_n	Adjustment range at the secondary side
DB	1% of V_n	Dead band
$\Delta V_{step\ tot}$	1.44 V	Voltage variation for each tap action
$D1$	60 ms	Delay-time before the tap action
$T_{step\ tot}$	60 ms	Time needed for the tap action
$P_{iron\ loss}$	15 W	Iron losses
$i_{0\%}$	0.18% of I_n	No-load current
$P_{Cu\ extreme}$	85 W	Copper losses at the extreme tap positions
$P_{Cu\ central}$	35 W	Copper losses at the central tap position
V_k	4% of V_n	Short-circuit voltage

3.2. Load – Modelling

As explained in Section 2.4, the utilized controllable load, although settable in terms of nominal active power, has an actual absorption characterized by a dependency to the square of the supply voltage. Therefore the load's physical behaviour is representable through a merely 'constant-impedance' unit.

Since in DIgSILENT PowerFactory software environment when running RMS simulations the standard load model is characterized by a 'constant-impedance' behaviour, the real load has been modelled through three generic passive single-phase load units. Appropriate load-events have been defined in order to obtain active power absorption changes, to reproduce the real activities performed during the tests.

3.3. EV – Modelling

The EV has been modelled through a generic load component characterized by negative values of power and current, so to obtain the correct power flow direction created by the discharging process of the battery. As explained in Section 2.5, as the utilized EV allows the manual setting of the discharging current, its physical behaviour needed to be represented through a merely 'constant-current' unit. Therefore, a realistic EV model has been built through a suitable correction block, aimed at guaranteeing the desired direct proportionality with the local voltage value. This feature has been obtained through an appropriate control scheme, where local voltage measurement and an external injection current profile provide the input signals V_{meas} [p.u.] and I_{file} [A] to a 'correction block', implementing (7), derived as reverse of (6).

$$P_{EV}=I_{file} \cdot V_0 \cdot (V_0/V_{meas})=P_{eff} \cdot (V_0/V_{meas})=P_0 \quad (7)$$

Since the real EV injects power with unitary power factor while providing V2G services, the reactive power Q_{EV} has been set constantly equal to 0.

4. Experimental and Simulation Activities

This section focuses on the evaluation of the real tap-changers activities and the implemented models. With the purpose of evaluating the modelled system, the results obtained from the practical tests are compared to the simulations' ones, by monitoring and calculating the same parameters and indexes.

4.1. Definition of Scenarios

With the purpose of monitoring the dynamics of the tap actions taking place as the consequence of a single-phase load changing, a preliminary test has been performed. In this regard, Scenario #0 has been

defined – see Table 2. It foresees the biggest possible single-phase (phase *c*) load increment occurring with a single event, i.e., a step from 0 kW to a loading condition of 11.6 kW. The other two phases' power flows remain unchanged. Phase *a* is affected by reverse power flow coming from the constant current injection of 16 A (corresponding to 3.4 kW) from the EV, while phase *b* is constantly loaded at 11.6 kW. This particular unbalanced condition has been chosen because it is relevant to analyse the single-phase tap action whenever the system is heavily stressed by reverse power flow and maximum loading condition.

Table 2 Scenario #0

	Phase *a* [kW]	**Phase *b* [kW]**	**Phase *c* [kW]**
Starting Condition	-3.4 (-16 A)	11.6	0
Ending Condition	-3.4 (-16 A)	11.6	11.6

Two more operative scenarios aim at verifying the decoupled-phase OLTC effectiveness under conditions characterized both by balanced/unbalanced conditions and different power flow directions on the three phases, while considering events on loads' power and EV's current injection. Specifically, Scenario #1 is mainly based on the consideration of balanced increases of power absorptions evenly by the three single-phase loads, by reason of 1 kW-steps from 0 kW to 11 kW every 3 minutes. The objective of Scenario #1 is the verification of appropriate operability of the three independent tap changers, in the case of balanced loads conditions, i.e., under a conventional power flow situation. In Table 3, the operation procedure and the actual single-phase set active power are reported.

Table 3 Scenario #1

Time of operation	**Phase *a* [kW]**	**Phase *b* [kW]**	**Phase *c* [kW]**
T=0s	0	0	0
T=28s	1.1	1.1	1.1
T=224s	2.2	2.2	2.2
T=390s	3.4	3.4	3.4
T=565s	3.7	3.7	3.7
T=751s	4.5	4.5	4.5
T=930s	5.6	5.6	5.6
T=1154s	6.7	6.7	6.7
T=1304s	7.8	7.8	7.8
T=1472s	9.3	9.3	9.3
T=1650s	10.8	10.8	10.8
T=1828s	11.6	11.6	11.6

For the second investigated operative scenario, the load on phase *a* has been replaced by the EV, while resistive single-phase loads have been maintained connected to phases *b* and *c*. Scenario #2 is thus characterized by increasing power injected by the EV, considering constant active power absorption (6.7

kW) on the other two phases. As at any considered situation the three phases are affected by different power flows in terms of both direction and loading, it is clear that the main objective of Scenario #2 is the analysis of the operations of the decoupled-phase OLTC in presence of different unbalanced situations and power flow directions. As described in Section 2.5, the VMS of the EV allows manual adjustment of the current. Considering this technical feature, the increase of the injected power at Scenario #2 has been obtained manually adjusting the current from 0 to 16 A with 2 A–steps every 3 minutes, reported in Table 4 in terms of active power.

Table 4 Scenario #2

Time of operation	Phase *a* [kW]	Phase *b* [kW]	Phase *c* [kW]
T=0s	-0.1 (-2 A)	0	0
T=48s	-0.1 (-2 A)	6.7	6.7
T=399s	-0.8 (-4 A)	6.7	6.7
T=560s	-1.3 (-6 A)	6.7	6.7
T=737s	-1.7 (-8 A)	6.7	6.7
T=915s	-2.1 (-10 A)	6.7	6.7
T=1097s	-2.6 (-12 A)	6.7	6.7
T=1277s	-3.0 (-14 A)	6.7	6.7
T=1457s	-3.4 (-16 A)	6.7	6.7

Graphical results are presented in terms of phase-neutral voltages both at the OLTC and the remote bus. For Scenario #2, in order to analyse the effects of unbalanced conditions, also the neutral-ground voltage at the remote bus has been monitored. Moreover, at either terminal of the cable, the voltage unbalance factor (VUF) has been calculated. Equation (8) describes the VUF, defined as the ratio between the negative and the positive voltage components in percent [26].

$$VUF_{\%}=V_{neg\_seq}/V_{pos\_seq} \cdot 100 \quad (8)$$

4.2. Results

4.2.1 Scenario #0: The results of Scenario #0 are reported in Fig. 6, where the tap operations from both the practical test and simulation activities are presented – named *V-c-Exp* and *V-c-Sim*, respectively. It can be noticed that in both cases the 11.6 kW-step load increase causes a voltage drop of roughly 11 V (i.e., 0.048 p.u.) and the time necessary to rise the voltage up within the dead band amounts to approximately 1 s. The dynamics of the tap actions, investigated in Section 2.3 and implemented in the simulation tool as described in Section 3.1, reflect the expectations. However, the model has some limitations due to the difficulty in perfectly characterizing the tap operation of the toroidal coil. As it can be appreciated in Fig. 6, the difference between the experimental measurements and the simulation results is kept within a narrow

range that can be considered acceptable, being the voltage deviations below 0.007 p.u. and the response time difference approximately equal to 40-60 ms. It has to be remarked that the measurement unit's accuracy is ± 0.1% of the voltage amplitude, while the sampling time is 20 ms.

This could lead to the conclusion that the implemented model could represent properly and realistically the real behaviour of the analysed OLTC.

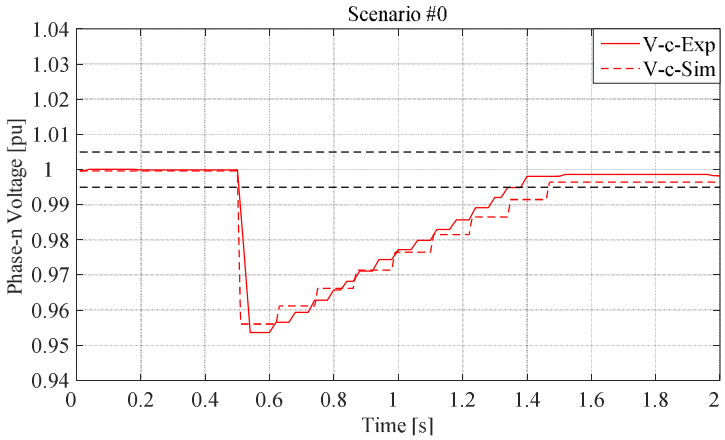

Fig.6. *Tap actions for phase c for Scenario #0*

4.2.2 Scenario #1: For each phase, the reference voltage V_{ref} (reported in Table 5) has been set in accordance with the voltage supplying the primary side, permitting to start the study with the tap selector at the '0-position' (unitary turns ratio). In order to compare efficiently the results, each phase-neutral voltage has been plotted in per unit, according to the respective V_{ref}.

Table 5 Voltage references for Scenario #1

V_{ref_a} [V]	V_{ref_b} [V]	V_{ref_c} [V]
233.6	233.9	234.4

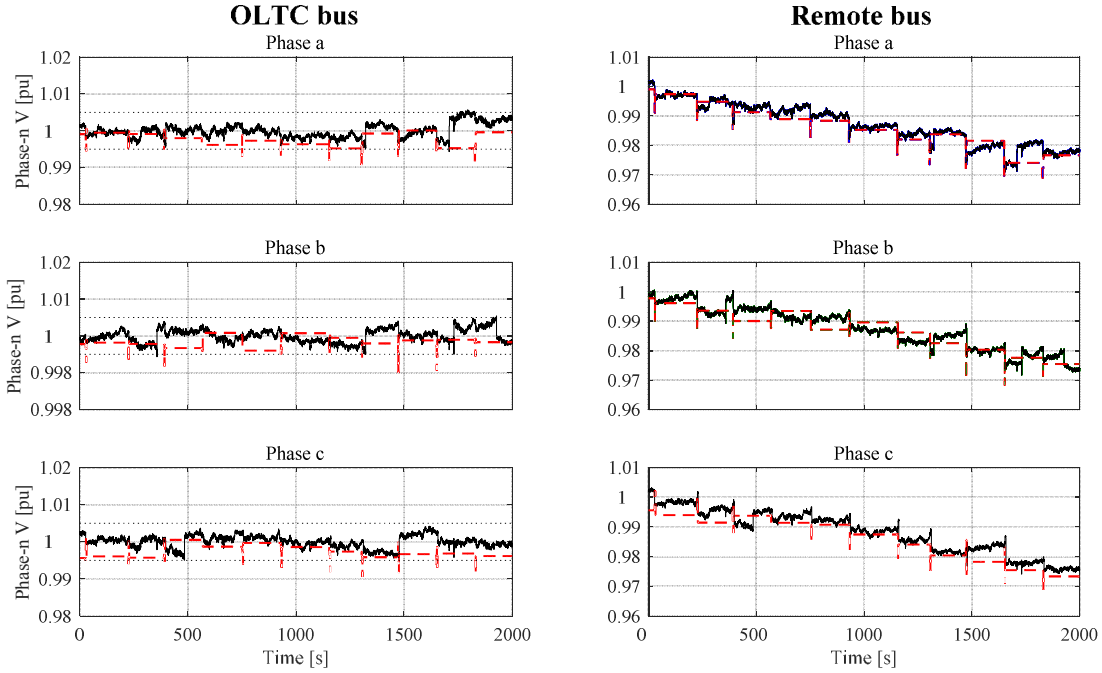

Fig.7. *Phase-neutral voltages for Scenario #1 at the OLTC and remote bus. The solid lines show the results from the experiments, the dashed ones from the simulations*

Fig. 7 shows the three phase-neutral voltages at the secondary side of the transformer and at the remote bus of the line. Comparisons of the results from the experimental test as well as the simulation study show that the modelled grid and components allow a realistic representation of the tested activities. In particular, from the plots on the left, it is possible to notice that, whenever one of the three phase-neutral voltages exceeds the lower allowed limit, a phase-independent tap action is performed. The plots on the right show that, since the OLTC controllers act based on local voltage measurements, voltages at the ending terminal bus are not considered in the control logic, being therefore characterized by increasing deviations from the nominal value, in accordance with the loads entity.

4.2.3 Scenario #2: For Scenario #2, V_{ref} have been manually set as reported in Table 6. Again, each phase-neutral voltage has been plotted in per unit, according to the respective V_{ref}.

Table 6 Voltage references for Scenario #2

V_{ref_a} [V]	V_{ref_b} [V]	V_{ref_c} [V]
230.7	230.5	230.1

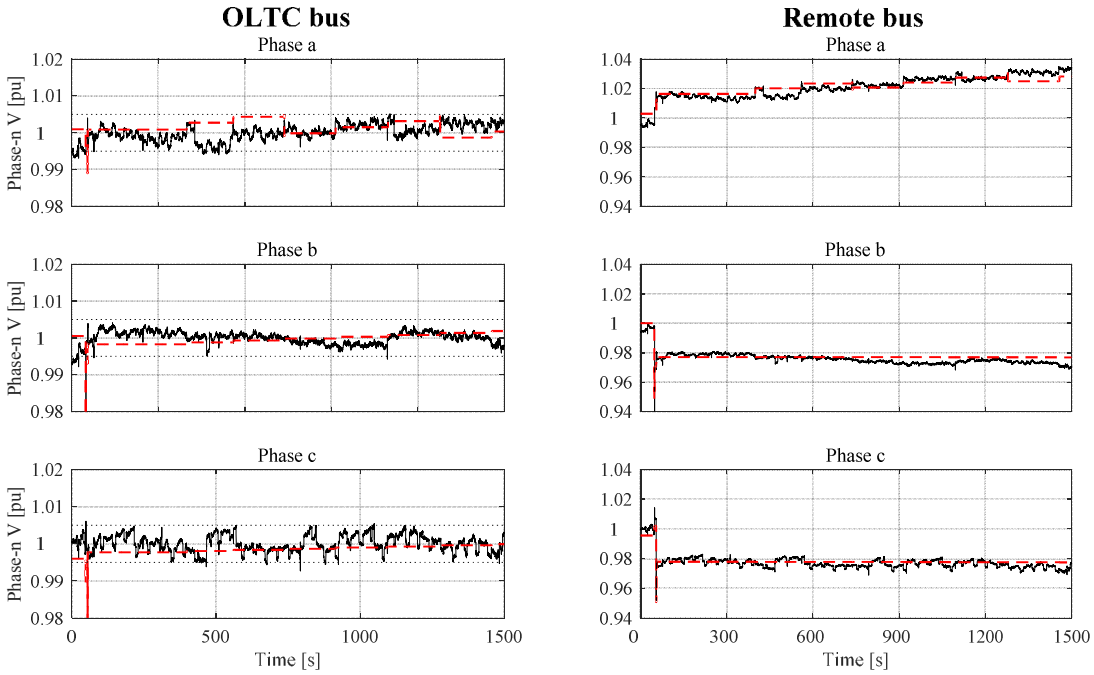

Fig.8. *Phase-neutral voltages for Scenario #2 at the OLTC and remote bus. The solid lines show the results from the experiments, the dashed ones from the simulations*

Fig. 8 shows the phase-neutral voltages at the two monitored points. In particular, from the plots on the left it is possible to notice that, due to a relevant load-step of 6.7 kW after 28 s, the phase-neutral voltages on phases *b* and *c* exceed the lower allowed limit dropping down to 0.97 p.u. (off the plot scale), leading to tap changing actions aiming at rising them within the dead band. The plots on the right show how voltages deviate differently on each phase at the remote bus: phase *a* presents an increasing voltage due to the increasing current injected by the EV, while phases *b* and *c* characterized by constant values after the cited initial reduction related to the load event.

From Table 7, it is noticeable that mean and maximum values of the neutral-ground voltage at the remote bus amount respectively to 1.92% and 2.51% of the rated voltage, both slightly higher than values obtained from the simulation. Regarding the VUF, its values at the remote bus are higher than those at the transformer level due to the higher voltage unbalance, making the negative sequence component more influent. It can also be noticed that values from the simulation at the OLTC bus are slightly higher than the real ones, while at the remote bus the results are very concordant in terms of mean values, below 2%. Difference of almost 1% has been found regarding the maximum value, which in the real test is even above 3%.

The imperfect match of experimental and simulation results, noticeable both from Table 7 and Fig. 8 (e.g., at t=~420 s, t=~1300 s), might be due to unavoidable continuous oscillations of the supply voltage at the primary side, which have not been possible to reproduce in the simulation study.

From figures 7 and 8, it is possible to notice that the experimental measurements present continuous oscillations during the whole operation, due to unavoidable and unpredictable fluctuations of the supply voltage provided by the external public grid. Such oscillations could not be reproduced within the simulation activities, thus justifying the not absolute match of the results. Due to these oscillations, the phase-neutral voltages do not exceed the thresholds exactly at the same moment, and therefore the tap actions do not take place perfectly simultaneously. Nevertheless, it is noticeable that overall the simulations reproduced the measurements very realistically, since the overall trends are emulated properly and the extent of the deviations is limited to maximum 0.007 p.u., which is an acceptable deviations when it comes to replication of power systems experiments.

Table 7 Neutral-ground voltage and VUF for Scenario #2

Activity	Neutral potential at remote bus		VUF at OLTC bus		VUF at remote bus	
	Mean Val.	Max Val.	Mean Val.	Max Val.	Mean Val.	Max Val.
Experimental	1.92%	2.51%	0.88%	1.54%	1.87%	3.16%
Simulation	1.66%	2.09%	1.42%	1.89%	1.85%	2.25%

5. Conclusions

This work presents both experimental and modelling activities of an OLTC transformer provided with single-phase-independent tapping capability, used to mitigate the increasing unbalanced conditions in distribution networks caused by the growing number of single-phase DERs. A detailed method aiming at a simplified representation of a real Danish LV distribution network is proposed: the obtained results allowed the choice of the components utilized for the tests, performed in the research infrastructure SYSLAB-PowerLabDK.

An investigation of the tap-changers' behaviour has been carried out and then modelled in DIgSILENT PowerFactory software environment. The comparison of the voltage trends showed that the proposed model allows a realistic representation of the real tap operation. Additionally, the OLTC's operability is studied in two scenarios characterized by both balanced and unbalanced load conditions as well as single-phase reverse power flow. From the experimental tests, it can be concluded that at the transformer level voltages have been maintained within the dead band, confirming the effectiveness of the tap operations, being the OLTC based on local measurements.

It is therefore proved that the investigated independent single-phase tap capability, instead of coordinated three-phase actions, mitigates voltage deviations, improving the distribution grid power quality.

Furthermore, comparisons of all the tested and simulated activities show that all the system components have been properly modelled, leading to the conclusion that the proposed models are reliable.

6. Acknowledgments

The authors acknowledge the financial support to this work given by the Danish EUPD program for the project Energy Saving by Voltage Management (ESVM), under the grant number 5996648995411.

7. References

[1] T. Stetz, M. Kraiczy, M. Braun, and S. Schmidt, “Technical and economical assessment of voltage control strategies in distribution grids,” Prog. Photovoltaics Res. Appl., vol. 21, no. 6, pp. 1292–1307, 2013.

[2] M. Braun, T. Stetz, R. Bründlinger, C. Mayr, K. Ogimoto, H. Hatta, H. Kobayashi, B. Kroposki, B. Mather, and M. Coddington, “Is the distribution grid ready to accept large-scale photovoltaic deployment? State of the art, progress, and future prospects,” Prog. photovoltaics Res. Appl., vol. 20, no. 6, pp. 681–697, 2012.

[3] R. Caldon, M. Coppo, and R. Turri, “Distributed voltage control strategy for LV networks with inverter-interfaced generators,” Electr. Power Syst. Res., vol. 107, no. 0, pp. 85–92, Feb. 2014.

[4] K. Knezović, M. Marinelli, R. J. Møller, P. B. Andersen, C. Træholt, and F. Sossan, “Analysis of Voltage Support by Electric Vehicles and Photovoltaic in a Real Danish Low Voltage Network,” in Proceedings of the 49th International Universities Power Engineering Conference (UPEC) IEEE, Cluj-Napoca, Romania, 2014.

[5] K. P. Schneider, J. C. Fuller, F. K. Tuffner, and R. Singh, “Evaluation of Conservation Voltage Reduction (CVR) on a National Level,” Pacific Northwest Natl. Lab., no. July 2010, p. 114, 2010.

[6] S. Rahimi, M. Marinelli, and F. Silvestro, “Evaluation of requirements for Volt/Var control and optimization function in distribution management systems,” IEEE Int. Energy Conf. Exhib. ENERGYCON, Florence, Italy, 2012, pp. 331–336, 2012.

[7] R. Uluski, “VVC in the Smart Grid Era,” IEEE PES General Meeting, Minneapolis, MN, 2010, pp. 1-7.

[8] M. S. Golsorkhi and D. Lu, “A Control Method for Inverter-Based Islanded Microgrids Based on V-I Droop Characteristics,” IEEE Trans. Power Deliv., vol. 30, no. 3, pp. 1196–1204, 2014.

[9] A. Kechroud, P. F. Ribeiro, and W. L. Kling, “Distributed generation support for voltage regulation: An adaptive approach,” Electr. Power Syst. Res., vol. 107, pp. 213–220, Feb. 2014.

[10] L. Carradore and R. Turri, "Electric Vehicles participation in distribution network voltage regulation," in 2010 45th International University Power Engineering Conference (UPEC), Cardiff, United Kingdom, 2010, pp. 1–6.

[11] C. Kumar and M. K. Mishra, "A voltage-controlled DSTATCOM for power-quality improvement," IEEE Trans. Power Deliv., vol. 29, no. 3, pp. 1499–1507, 2014.

[12] A. Einfalt, F. Kupzog, H. Brunner, and A. Lugmaier, "Control strategies for smart Low voltage grids – the project DG DemoNet – smart LV grid," in Integration of Renewables into the Distribution Grid, CIRED 2012 Workshop,Lisbon, Portugal, 2012, no. 0238, pp. 1–4.

[13] I. Leisse, O. Samuelsson, and J. Svensson, "Coordinated voltage control in medium and low voltage distribution networks with wind power and photovoltaics," in IEEE PowerTech Conference, Grenoble, France, 2013, pp. 1–6.

[14] M. S. El Moursi, H. H. Zeineldin, J. L. Kirtley, and K. Alobeidli, "A dynamic master/slave reactive power-management scheme for smart grids with distributed generation," IEEE Trans. Power Deliv., vol. 29, no. 3, pp. 1157–1167, 2014.

[15] "GRIDCON® TRANSFORMER - Datasheet." Maschinenfabrik Reinhausen Gmbh, online available - http://www.reinhausen.com/en/desktopdefault.aspx/tabid-1605/1835_read-4652/.

[16] "FITformer® REG - Datasheet." Siemens, online available - http://www.energy.siemens.com/hq/en/power-transmission/transformers/distribution-transformers/distribution/fit-former-reg.htm.

[17] W. Sinsukthavorn, E. Ortjohann, A. Mohd, N. Hamsic, and D. Morton, "Control Strategy for Three/Four-Wire-Inverter-Based Distributed Generation," IEEE Trans. Ind. Electron., vol. 59, no. 10, October, pp. 3890–3899, 2012.

[18] B. Meersman, B. Renders, L. Degroote, T. Vandoorn, and L. Vandevelde, "Three-phase inverter-connected DG-units and voltage unbalance," Electr. Power Syst. Res., vol. 81, no. 4, pp. 899–906, Apr. 2011.

[19] J. Hu, M. Marinelli, M. Coppo, A. Zecchino, and H. W. Bindner, "Coordinated voltage control of a decoupled three-phase on-load tap changer transformer and photovoltaic inverters for managing unbalanced networks," Electr. Power Syst. Res., vol. 131, pp. 264–274, 2016.

[20] A. Zecchino, M. Marinelli, J. Hu, M. Coppo, and R. Turri, "Voltage Control for Unbalanced Low Voltage Grids Using a Decoupled-Phase On-Load Tap-Changer Transformer and Photovoltaic Inverters," in 50th International Universities Power Engineering Conference, Stoke-On-Trent, United Kingdom, 2015, pp. 1–6.

[21] "Automatic Voltage Stabilizer - Datasheet." Schuntermann Transformatoren Gmbh, online available - http://www.renecost.de/wp-content/uploads/2015/02/Spannungskonstanthalter_290414.pdf.

[22] "SYSLAB-PowerLabDK." [Online]. Available: http://www.powerlab.dk/facilities/syslab.aspx.

[23] ELSPEC, "G4500 & G3500 Portable Power Quality Analyzer USER & INSTALLATION MANUAL." V1.2 SMX-0618-0100, 2013.

[24] W. W. Price, "IEEE Task Force on Load Representation for Dynamic Performance, Load representation for dynamic performance analysis," IEEE Trans. Power Syst., vol. 8, no. 2, pp. 472–482, 1993.

[25] S. Martinenas, M. Marinelli, P. B. Andersen, and C. Træholt, "Implementation and demonstration of grid frequency support by V2G enabled electric vehicle," in Proceedings of the 49th International Universities Power Engineering Conference (UPEC) IEEE, Cluj-Napoca, Romania, 2014, pp. 1–6.

[26] P. Pillay and M. Manyage, "Definitions of voltage unbalance," IEEE Power Eng. Rev., vol. 22, no. 11, pp. 49–50, 2002.